Chapter 4
Stress Concentration Evaluation of a Plate with Symmetrical U-Notches Under Tensile Load Using TSA and a Lepton IR Camera

V. E. L. Paiva, D. G. G. Rosa, G. L. G. Gonzáles, and J. L. F. Freire

Abstract It has already been showed that Thermoelastic Stress Analysis (TSA) may be employed as an extremely useful technique in structural integrity assessment applications. Recent developments in the microbolometer technology made possible the commercial offer of very low-cost infrared cameras, one of these being the FLIR Lepton 3.5. Use of such low-cost cameras associated with commercially available software or in-house developed algorithms makes possible to localize anomalies and to determine quantitative results on the stress distribution acting on nominal and hot-spot locations in loaded structures. A further step will widely disseminate IR temperature and TSA measurements and consequent analyses into a powerful low-cost health monitoring tool. The aim of the present work is to demonstrate the use of this experimental technique in the evaluation of the stress concentration caused by a U-notch in a plate under tension load using TSA and a Lepton camera. A MATLAB in-house algorithm was developed for post-processing the measured IR signal. The achieved stress-distribution and stress-concentration results are also compared with those generated by measurement systems that integrate a commercially available software coupled to the FLIR Lepton 3.5 and to a median-cost FLIR A655sc IR camera. Moreover, the paper shows that the low-cost camera can be used in the monitoring of fatigue crack growth as well as in the determination of stress intensity factors for cracks initiated and propagated from the U-notch.

Keywords Thermoelastic stress analysis · TSA · Lepton 3.5 · Stress concentration

4.1 Introduction

Discontinuities or abrupt geometric changes in a loaded structure act as stress raisers and cause high localized stresses [1] that may fatigue damage.

Fatigue is one of the most common cause of mechanical failure in engineering components and its prevention is a major concern in structural health [2, 3]. Fatigue cracks commonly initiate at stress concentration features such as imposed designed abrupt geometric changes, initial damage caused by some manufacturing processes, or external third-order interference and can propagate during continuous operation, not necessarily causing an imminent risk, but surely impairing its functionality, accelerating its degradation, and diminishing its service life.

The use of infrared (IR) thermography, more specifically thermoelastic stress analysis (TSA) [4], as a nondestructive evaluation (NDE) technique to analyze the behavior cyclic load components is not new, being used in large scale to evaluate the delamination of composite polymer materials [5–7], crack inspection [8–12], and estimation of remaining strength of components [13–17], playing an important role in maintenance programs and in-service inspections.

In recent years, new developments in the technology of the microbolometer have enabled the emergence of very low-cost thermal camera models, such as the Lepton one. However, these low-cost models offer reduced capabilities as compared to high-end devices mainly due to the sensor spatial resolution, simpler optics, housing, and electronics. The quality of the achieved results is proportional to the investment in the sensor; nevertheless, the possibilities of application to structural health monitoring are countless [18, 19].

The present paper presents the application of the TSA technique to analyze the stress concentration generate by a U-notch in a polycarbonate plate under tension using a low-cost Lepton camera. The IR signal was post-processed using a MATLAB

V. E. L. Paiva (✉) · G. L. G. Gonzáles · J. L. F. Freire
Department of Mechanical Engineering, Pontifical Catholic University of Rio de Janeiro, PUC-Rio, Greece

D. G. G. Rosa
Department of Civil Engineering, Rua Marquês de São Vicente, Rio de Janeiro, RJ, Brazil

S. L. B. Kramer et al. (eds.), *Thermomechanics & Infrared Imaging, Inverse Problem Methodologies, Mechanics of Additive & Advanced Manufactured Materials, and Advancements in Optical Methods & Digital Image Correlation, Volume 4*, Conference Proceedings of the Society for Experimental Mechanics Series, https://doi.org/10.1007/978-3-030-86745-4_4

algorithm. The results were compared with those generated by measurement systems that integrate a commercially available software coupled to the FLIR Lepton 3.5 and to a median-cost FLIR A655sc IR camera. Digital image correlation system (DIC) and finite element method (FEM) were also employed for additional evaluation and comparison. Moreover, the paper shows that the low-cost camera can be used in the monitoring of fatigue crack growth as well as in the determination of stress intensity factors for cracks initiated and propagated from the U-notch.

4.2 Material and Experimental Procedure

The material analyzed in this work was polycarbonate, which is a well-balanced material with relatively high resistance to temperature, ductility, and both mechanical and impact strengths. For this reason, it is generally considered an engineering plastic and has multiple applications.

Two types of specimens were used herein, both made of the same polycarbonate sheet. The first one was a dog bone specimen, also known as the constant radius tensile specimen, presenting a smooth stress gradient along its length due to the continuous variation of the cross-sectional area. The uniaxial tensile stress-strain curve for the material, Fig. 4.1, was determined using DIC to measure the displacement full-field while the dog bone specimen was monotonic loaded until failure. Further relevant material data are given in Table 4.1. It is relevant to notice at this point that the stress-strain curves used the minimum cross section dimensions for stress calculation and that the strain data was determined by a long virtual gage as depicted in Fig. 4.1. No attempt was made to determine equivalent strains from the triaxial strain state after the occurrence of necking, meaning that the stress-strain curves and presented mechanical property data are accurate up to the point where stresses reach their peak.

The DIC used hardware was composed of a tripod and fixtures to adapt two 2.3 megapixel CMOS cameras (Basler acA1920-155um) coupled to adjustable focal length lenses (Tamron A031 AF28-200 mm F/3.8–5.6). A calibration target (12 × 8 dots with 15 mm of grid spacing) compatible with the DIC Vic Snap and VIC-3D software (Correlated Solutions Inc.) was used for calibration.

The second type of specimen and main object of the present analysis was a bar with symmetrical and opposite U-shaped notches (thickness = 2.94 mm, width = 49.96 mm, length = 250 mm and notch radius = 9.33 mm), Fig. 4.2a. The specimens were tested in a 100kN INSTRON servo-hydraulic machine under cyclic axial load ($R = \sigma min/\sigma max = 0.1$ and $f = 1$ Hz).

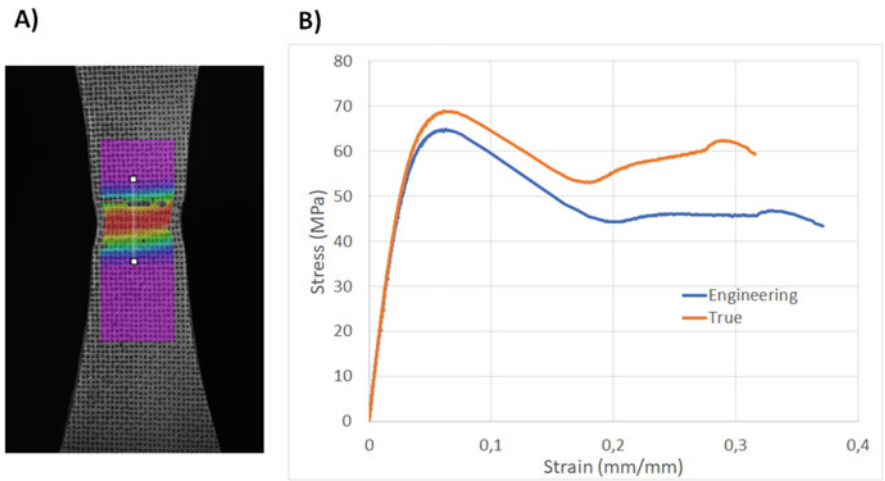

Fig. 4.1 Uniaxial tensile test: (**a**) Axial trains measured in the dog bone specimen using DIC during the test; (**b**) polycarbonate true and engineering stress-strain curves (accurate up to the stress peak)

Table 4.1 Polycarbonate engineering properties

Young's modulus	2039 MPa
Poisson's coefficient	0.42
Yield strength 0.2%	47 MPa
Ultimate (peak) strength	69 MPa
Infrared emissivity	0.9

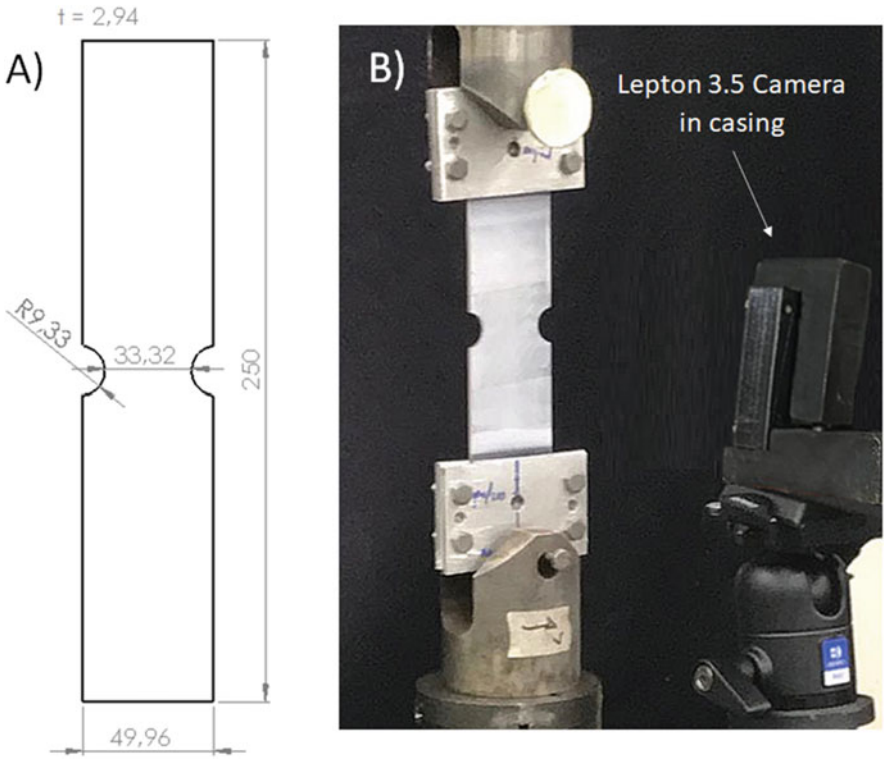

Fig. 4.2 U-notch strip: (**a**) Strip geometry, dimensions in mm; (**b**) Experimental setup

Figure 4.2b presents the experimental setup. The U-notch bar fatigue test was performed with a maximum load of 1.80 kN and a minimum of 0.18 kN, equivalent to a uniaxial nominal-net stress range of 16.5 MPa. This value is above the fatigue limit determined in [20] equal to 13.8 MPa for $N = 10^5$ cycles.

During each cyclic test, the surface temperature of the specimens was recorded in real time by two different thermal cameras: a low-cost FLIR Lepton 3.5 [21] (160 × 120 pixels resolution uncooled microbolometers, 8.7 Hz acquisition rate and <50 mK sensitivity) and a medium-cost FLIR A655sc camera [22] (640 × 480 pixels resolution uncooled microbolometers, up to 50 Hz acquisition rate, 30 mK sensitivity).

For each camera, two different approaches were taken. One approach worked with temperature data analyzed with the Stress Photonics' DeltaTherm II software [23] (using constant amplitude mode and intervals of 2 s for accumulation time and 32 seconds for integration time). The other approach worked with temperature data analyzed with the FLIR's ResearchIR software (for the medium cost-camera) or with the Parabilis Thermal Imaging software [24], which used a Raspberry Pi 4 Model B and a PureThermal 2 Smart I/O Module (for the low-cost Lepton 3.5 camera). In this second approach the measured raw temperature data was post-processed using a MATLAB in-house developed algorithm.

Parabilis Thermal Imaging is an open-source software that runs on a computer with a Linux-based operating system, which can be a desktop or, in this case, a Raspberry Pi computer. The Lepton camera was integrated into the Purethermal board adapting I/O camera pins to the USB interface.

The developed MATLAB algorithm used the least square method to fit the measured values of temperature variation (ΔT), which were obtained from the thermal images captured with both thermal cameras. The algorithm was designed to estimate the test frequency (under cyclical loading conditions) from the temperature fitting process. During all tests the Lepton camera was set up with the maximum acquisition rate of 8.7 fps, while the A655sc camera used an acquisition rate of 50 fps for the Deltatherm software approach and 8.7 fps for the MATLAB algorithm approach.

The TSA signal in the in-house algorithm was integrated over 278 frames with an accumulation time of 2 s, equivalent to approximately 32 s of collection time, meaning that a total of 278 frames were collected and then processed with an interval of 2 s to form a single TSA image, the results representing the average of 16 images combined.

The finite element method was used to assess the behavior of the U-notched strip specimen under load. A model consisting of 37,590 elements (SOLID186-SURF154-COMBIN14) and 191,169 nodes, Fig. 4.3, was constructed using a commercial package ANSYS v18.1 to simulate the stress state around the notches and the crack initiation and propagation. The continuous-line true-stress-true strain curve depicted in Fig. 4.1b was inputted in the numerical model. A 1.62 kN uniaxial

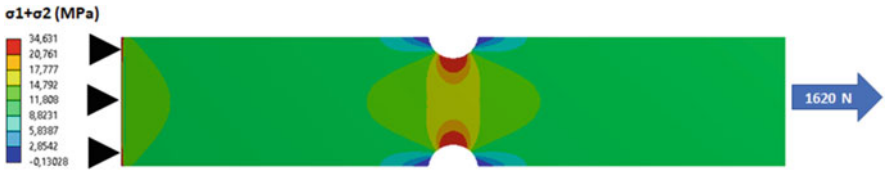

Fig. 4.3 U-notch strip finite element model loaded by a uniaxial 1.62 kN force and resulting invariant (σ1 + σ2) stress distribution

force equivalent was applied in one of the ends while the displacements of the other end were restrained. Moreover, the model was also subjected to a series of loads for validation via DIC comparison.

In addition, prior to the uniaxial tensile test the dog bone specimen was used for a calibration analysis between the measured temperature variations and the cameras response signal.

4.3 TSA Signal Calibration

To correlate the cyclic invariant stress range with temperature range, it is necessary to quantify the gain from the thermoelastic signal [4] by means of a calibration process. For this purpose, several tests were performed on specimens with known stress states ($\Delta\sigma 1 + \Delta\sigma 2$).

Using the dog bone specimen uniaxially loaded, $\Delta\sigma 1 = \Delta F/A$ and $\Delta\sigma 2 = 0$, where ΔF is the applied load range and A is the cross section being analyzed. A series of tests was carried out with uniform stress amplitudes actuating in the smallest cross section of specimen equaling 5, 10 15, 20, and 25 MPa. The used load ratio (R) was equal to 0.1.

Figures 4.4 and 4.5 present the post-processed TSA magnitude values for both approaches and both cameras for the tested loads, respectively, for the A655sc and Lepton 3.5 camera. The left images show the magnitude values measured using the in-house algorithm while the right images show the values obtained with the Deltatherm II software. The results for the TSA magnitude values are displayed in °C for the in-house algorithm and in camera units for the Deltatherm II software.

Figure 4.6 shows the relationship between the applied stress amplitude at the smallest cross section of the dog bone specimen and the corresponding TSA magnitude response, the results for in-house algorithm at left and right for the Deltatherm 2 software. The high noise data originated from low stress amplitudes measured with the Lepton camera were disregarded from the analysis.

4.4 Results and Discussion

This section presents results determined with the TSA technique using both cameras compared with DIC and or FE results. The presented results encompass stress distributions, stress concentration factors, and stress intensity factors for cracks that originated from the notches during the cycled tests.

4.4.1 Stress Distribution and Stress Concentration Results

Finite element and DIC techniques provided relevant information about full-field stress and strain distributions actuating in the U-notch strip specimen as presented in Fig. 4.7. It was found a good agreement between displacement and strain results measured by the DIC and determined from the FE model for the positions located at the notches, also known as hot spots. Figure 4.7 shows the principal strain results for a load equal to 1kN.

The TSA magnitude outputs (proportional to the elastic principal stress-invariant ranges) for the U-notch strip using the two cameras and two processing approaches are presented in Fig. 4.8. The hot spots are located at the edge of the notches, positions that experience greater stress ranges and consequentially greater temperature variations.

The relation between the TSA magnitude signal and the principal stress state was made using the linear calibration relationships given by the slopes of the tendency lines depicted in Fig. 4.6. DIC, FEM, and TSA results determined along the meridional line that passes through the center of the specimen, going from one notch to another as shown in Fig. 4.7, are

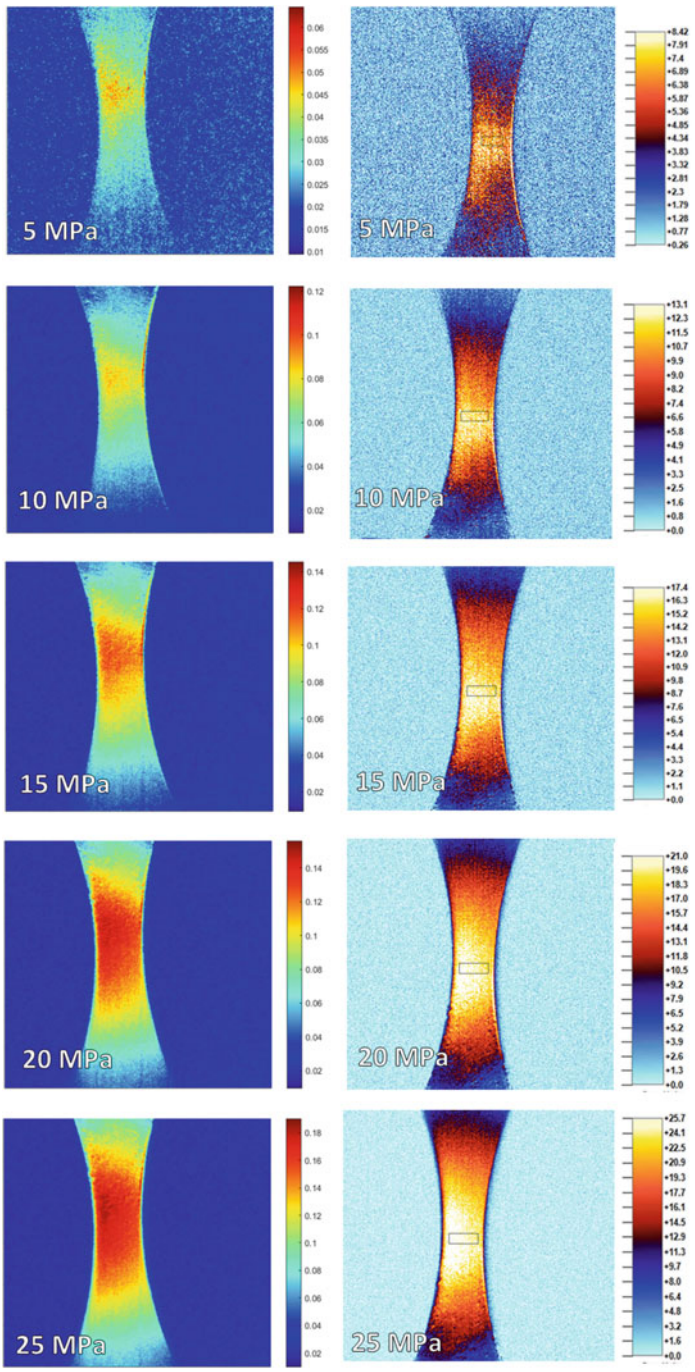

Fig. 4.4 Measure values of TSA magnitude using the FLIR A655sc camera: in-house algorithm (left column), Deltatherm II software (right column)

plotted in Fig. 4.9 in terms of the sum of the principal stress for an alternate load equal to 1.62 kN. Although some discrepancy exists, results showed very good comparison among the TSA, the DIC, and the FE results.

The TSA signal is composed of a magnitude proportional to the temperature variation caused by the thermoelastic effect, and a phase angle, which is related to the signal of the actuating stresses. Vieira et al. [25] studied fatigue crack propagation on a SAE keyhole specimen made of polycarbonate, finding and defining a phase angle modulus equal to 45^0 to differentiate the magnitude signal (tension or compression). This value was found based on the specimen geometry and expected behavior. In

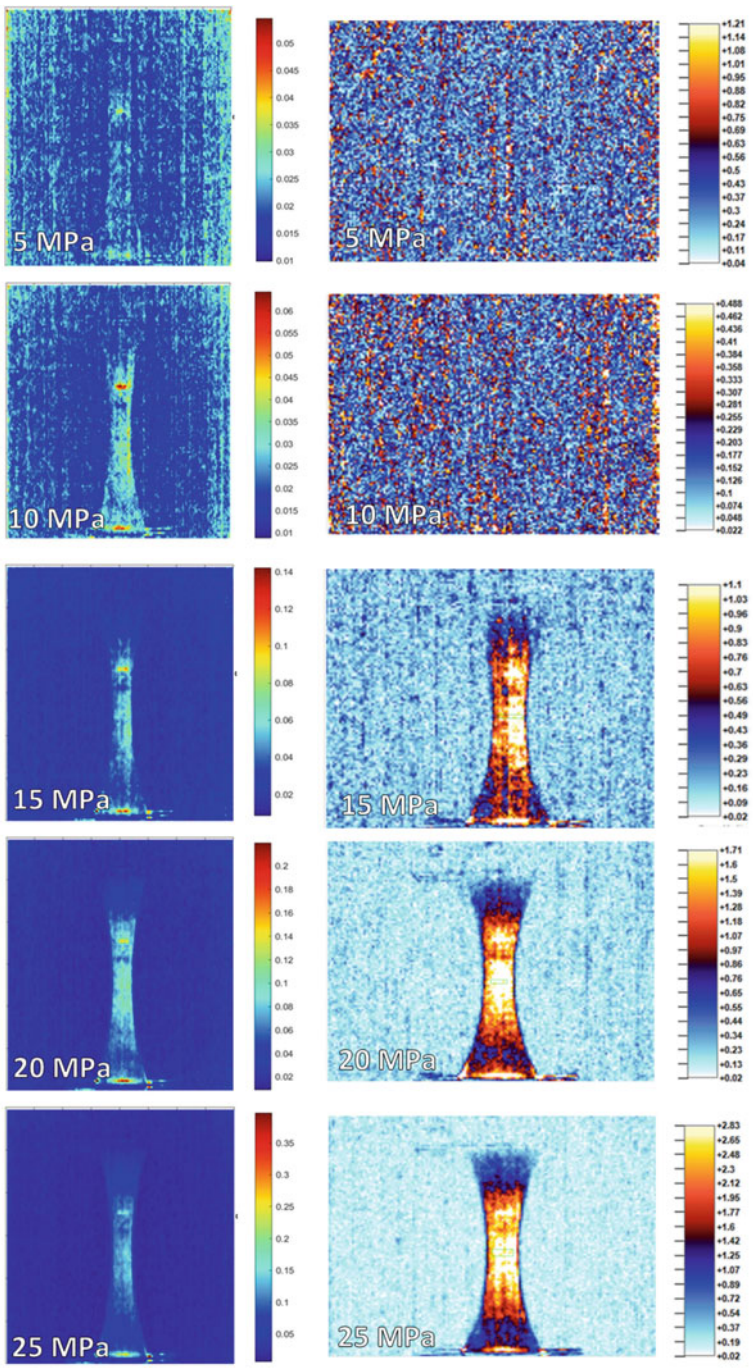

Fig. 4.5 Measure values of TSA magnitude using the FLIR Lepton 3.5 camera: in-house algorithm (left column), Deltatherm II software (right column)

the present paper all TSA measured ranges were positive, the phase angle approaching to zero degrees, in accordance with the determined stress results determined using the DIC and FE techniques.

The stress/strain concentration factors (defined using the gross nominal section) corresponding to both U-notches were measured and estimated using the experimental and numerical techniques. These values are shown in Table 4.2.

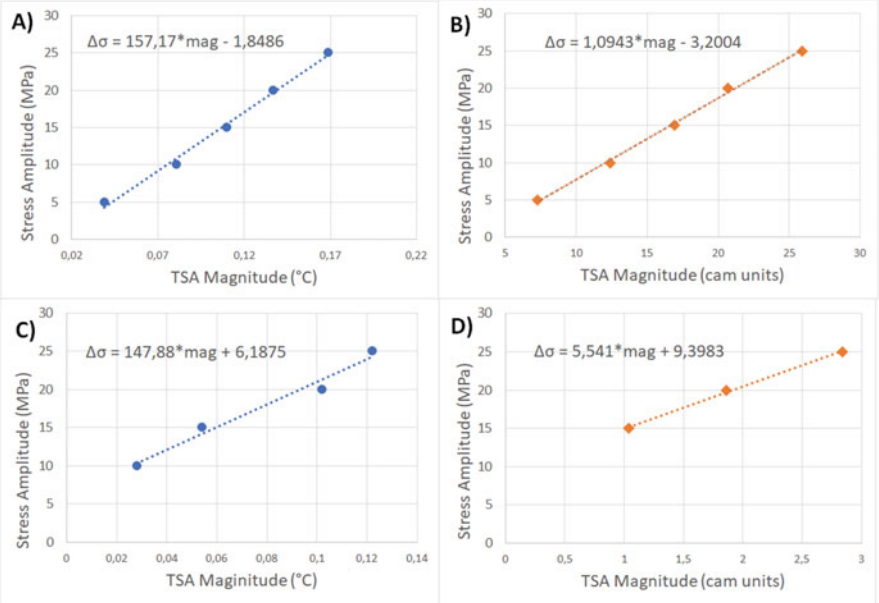

Fig. 4.6 Relationship between applied stress amplitude with TSA magnitude response: (**a**) in-house algorithm FLIR A655sc; (**b**) Deltatherm II FLIR A655sc; (**c**) in-house algorithm FLIR Lepton 3.5; (**d**) Deltatherm II Lepton 3.5

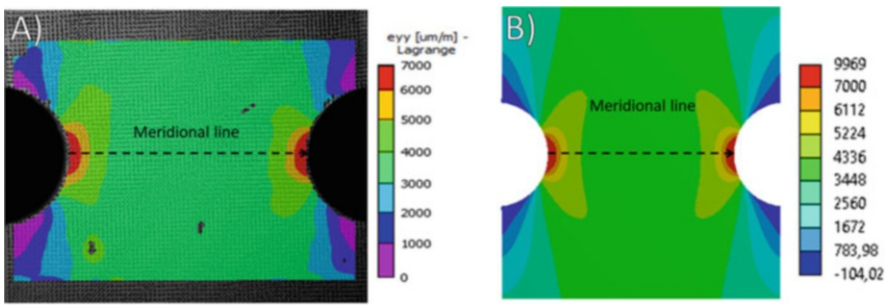

Fig. 4.7 U-notch strip specimen principal strain results for a load equal to 1kN: a) DIC; b) FEM

4.4.2 Stress Intensity Factor Results

While TSA is in essence a linear elastic technique, some plasticity occurs in and around hot spot positions and consequently fatigue cracks may be initiated after a considerable number of load cycles. Due to the nature of the technique, it can be used to locate, monitor the development of a fatigue crack, and furnish quantitative information on the stress intensity factor [25, 26]. Therefore, besides providing information on the stress state of a cyclic loaded sample, TSA can also be extended as a fatigue monitoring tool, supplying real-time information about the specimen damage condition.

The birth and evolution of fatigue crack is accompanied by a local stress relief, which is perceived as the decrease in the stress level compared to an earlier stage. Large cracks can be easily spotted, while small ones need several cycles until can be detected [27]. If the crack is already present in the specimen or the measurement begins after its development, it can be identified by the stress concentration originated at the crack tip and the stress relief along the crack surfaces.

As already noticed using data from the FLIR camera in previous publications [13–15, 27], the present TSA monitoring of the U-notch specimen with the Lepton camera helped to detect an increase in the stress level in the right notch of the specimen, symbolizing the initiation and start of propagation of a fatigue crack. Thereafter, the crack existence becomes noticeable in 856 cycles. Figure 4.10 shows a sequence of images where becomes evident the growth of a crack in the hot-spot area.

Different approaches have been developed to estimate stress intensity factor ranges (ΔK) from the analysis of the TSA response [4, 26, 28]. The data at the tip of the crack and very close to it tend to be very noisy due the presence of plasticity and high stress gradients. Treatment of the TSA data near the crack tip such as suggested by the Stanley's method [30] uses the first two terms of the Westergaard's stress function to adjust the thermoelastic data around the cracks in modes I and II. The

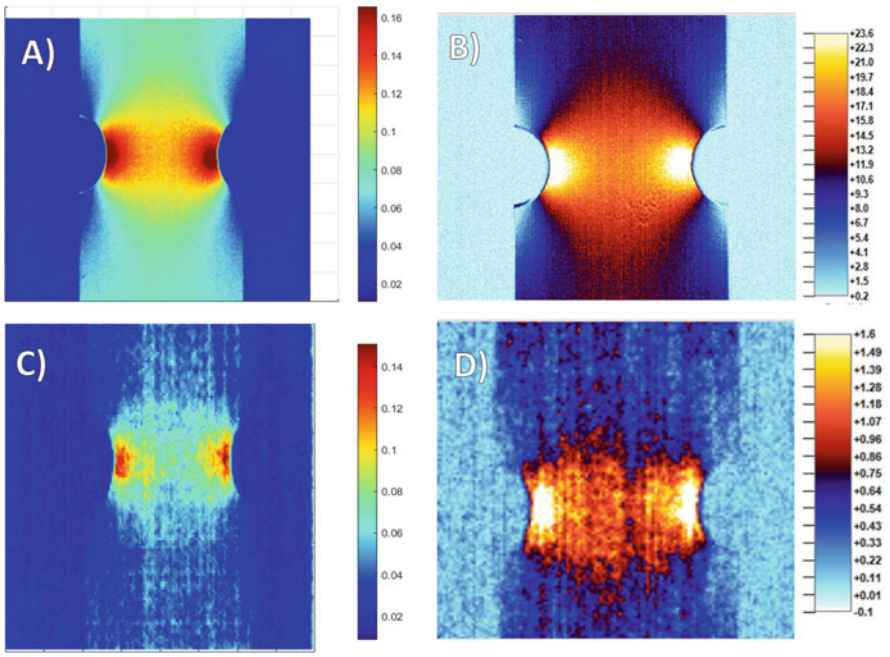

Fig. 4.8 TSA magnitude of the U-notch strip specimen: (**a**) in-house algorithm with FLIR A655sc camera; (**b**) Deltatherm II with FLIR A655sc camera; (**c**) in-house algorithm with FLIR Lepton 3.5 camera; (**d**) Deltatherm II with FLIR Lepton 3.5 camera

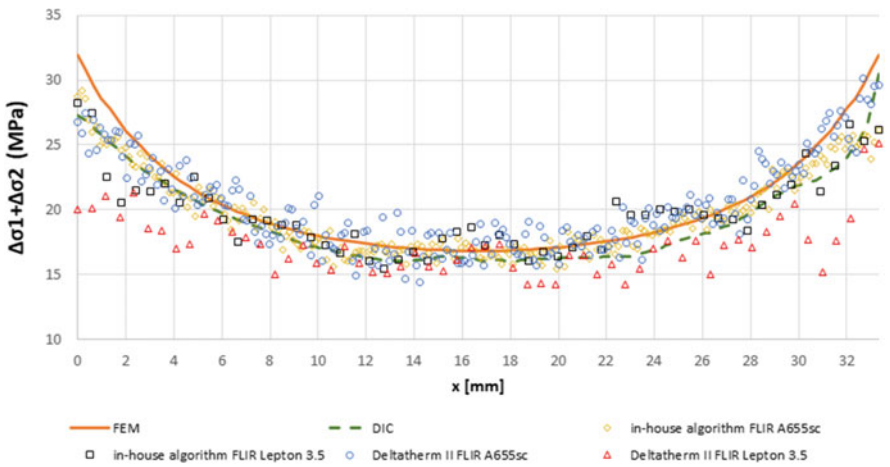

Fig. 4.9 Sum of the principal stress along of the meridional line of the U-notch strip for different techniques

Table 4.2 Stress/strain concentration factors corresponding to both U-notches

	Stress/strain concentration factor	
Method	Left notch	Right notch
FEM	2.87	2.87
DIC	2.88	2.97
In-house algorithm FLIR A655 sc	2.86	2.80
In-house algorithm FLIR lepton 3.5	2.85	2.86
Deltatherm II FLIR A655 sc	2.85	2.94
Deltatherm II FLIR lepton 3.5	2.52	2.85
Analytical Formulation [1]	2.95	2.95

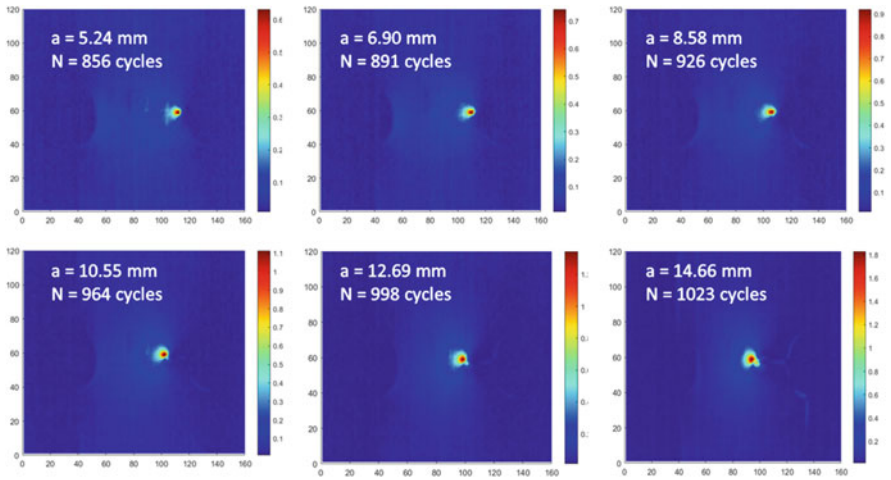

Fig. 4.10 Fatigue crack propagation on the right notch of the U-notch strip

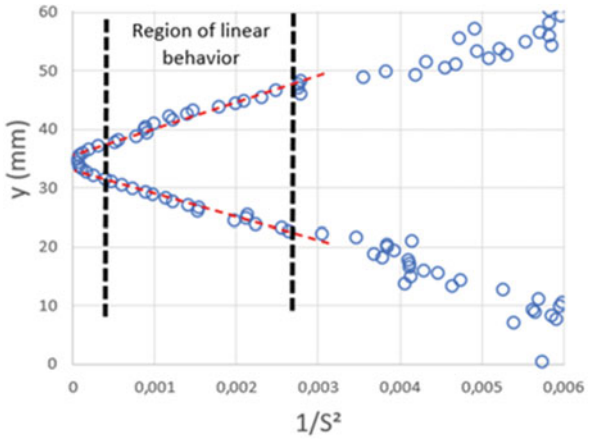

Fig. 4.11 Relationship between the vertical distance from the crack tip and ($1/S^2$) employed in the methodology of Stanley for the calculation of ΔK using TSA for the U-notch specimen with a 12.69 mm crack

method is only valid for the region of elastic and linear behavior near the crack tip and uses the gradient of this region to calculate ΔK. This method was applied herein.

Figure 4.11 presents points given by pair of coordinates where the horizontal axis' values are calculated using the inverse square of the TSA signal ($1/S^2$) plotted and the ordinate values are given by the vertical distance (y) to the crack. The Stanley's method uses Eq. (4.1) to determine ΔK as a function of the slope of the of the dashed line presented in Fig. 4.11.

$$\Delta K_{TSA} = \sqrt{4\pi \cdot A^2 \cdot tan\ \alpha / \left(3\sqrt{3}\right)} \tag{4.1}$$

where tan α is the slope of the y distance versus $1/S^2$ and A is the material calibration constant.

A crack was propagated in Mode I along the meridional line of the tested specimen, starting from the right U-notch. Crack lengths were measured with a caliper while TSA data were being collected. With a spatial resolution of 0.55 mm per pixel from the Lepton camera, stress intensity factors in mode I were calculated using the TSA-Stanley's approach and are compared with FEM determined ΔK results, which were based on an approach described in reference [29]. Results from this comparison are presented in Fig. 4.12.

Figure 4.13 presents plots of crack growth rate against the actuating stress intensity factor in mode I calculated using the TSA signal measured with the Lepton camera. These experimentally determined results were compared with the calculated FEM numerical results and show good agreement.

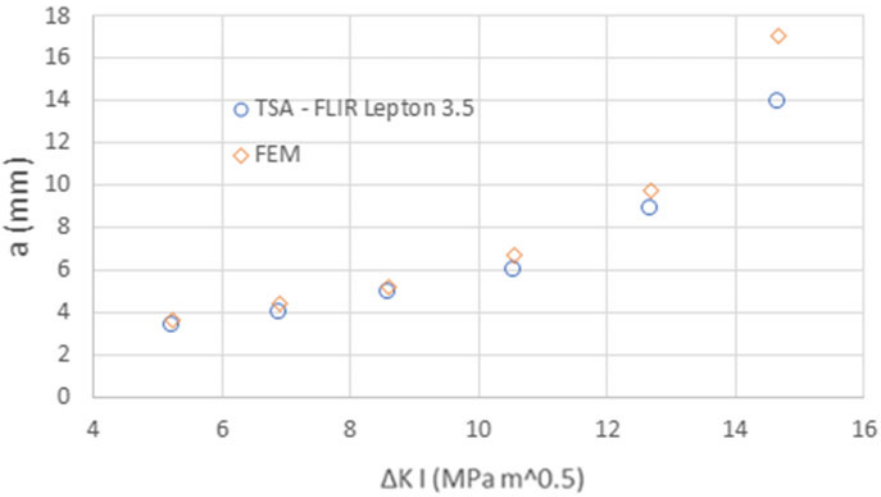

Fig. 4.12 Stress intensity factors in mode I for various crack lengths calculated using FEM and the Stanley's method based on the TSA signal measured with the FLIR Lepton camera

Fig. 4.13 Stress intensity factors in mode I plot against the crack growth rate using TSA signal measured with the Lepton camera and FEM

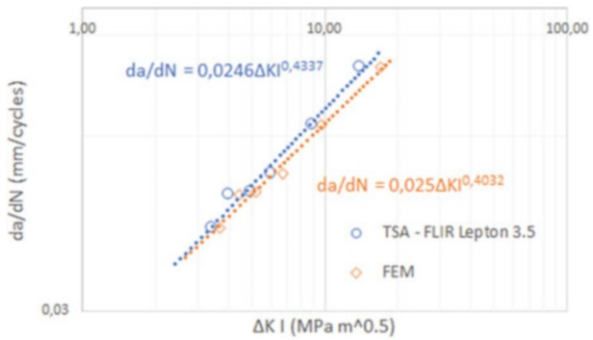

4.5 Conclusions

It has been showed along the years that TSA is a powerful tool for monitoring and evaluating structural health. Further advances in thermal camera technology have enabled much less inexpensive models, such as FLIR Lepton 3.5, to emerge, making it more accessible to be used in stress analysis. Although the quality of the results may be seen proportional to the investment in the camera, such low-cost cameras may be used as efficient alternatives for stress and damage monitoring in structures, mainly when large number of points need to be monitored considering affordable cost restrictions.

The present paper combines a set of different experimental and numerical techniques to assess the stress distributions and monitor fatigue damage of a U-notch specimen made of polycarbonate. DIC and FEM were used to provide relevant data about the stress/strain state at the notches area. Furthermore, the TSA technique was applied using a low-cost Lepton camera and a medium-cost FLIR A655sc camera. Data analysis used two different approaches: an in-house developed MATLAB algorithm and the commercial software Deltatherm II.

The results obtained using the Lepton camera were similar to those measured and obtained in other ways. The determined stress concentration factors at the hot spots presented good agreement among the applied experimental and numerical techniques. Another two objectives were achieved by showing that crack initiation and crack growth could be monitored using the low-cost camera as well as that stress intensity factors could also be accurately measured, therefore anticipating promissory applications of TSA in the integrity assessment of actual structures and their components.

References

1. Peterson, R.E., Plunkett, R.: Stress concentration factors. J. Appl. Mech. **42**(1), 248 (1975)
2. Anderson, T.L.: Fracture Mechanics: Fundamentals and Applications. CRC Press, New York (2017)
3. Castro, J.T., Meggiolaro, M.A.: Fadiga - Técnicas e Práticas de Dimensionamento Estrutural sob Cargas Reais de Serviço, 2nd edn. CreateSpace, Scotts Valley (2009)
4. Greene, R.J., Patterson, E.A., Rowlands, R.E.: Thermoelastic stress analysis. In: Sharpe, W.N. (ed.) Springer Handbook of Experimental Solid Mechanics, pp. 743–767. Springer, Berlin (2008)
5. Sirca, G.F., Adeli, H.: Infrared thermography for detecting defects in concrete structures. J. Civ. Eng. Manag. **24**, 508–515 (2018)
6. Avdelidis, N.P., Hawtin, B.C., Almond, D.P.: Transient thermography in the assessment of defects of aircraft composites. NDT & E Int. **36**, 6 (2003)
7. Sakagami, T., Komiyama, T.: Thermographic nondestructive testing for concrete structures. J JSNDI. **47-10**, 723–727 (1998)
8. Sakagami, T., Kubo, S.: Development of a new crack identification method based on singular current field using differential thermography. SPIE Proc. **3700**, 369–376 (1999)
9. Sakagami, T., Kubo, S., Teshima, Y.: Fatigue crack identification using near-tip singular temperature field measured by lock-in thermography. Proc SPIE. **4020**, 174–181 (1999)
10. Sakagami, T., Nishimura, T., Kubo, S.: Development of a self-reference lock-in thermography and its application to crack monitoring. Proc. SPIE. **5782**, 379–387 (2005)
11. Sakagami, T.: Remote nondestructive evaluation technique using infrared thermography for fatigue cracks in steel bridges. Fatigue Fract. Eng. Mater. Struct. **38**, 755–779 (2015)
12. Sakagami, T., Mizokami, Y., Shiozawa, D., Fujimoto, T., Izumi, Y., Hanai, T., Moriyama, A.: Verification of the repair effect for fatigue cracks in members of steel bridges based on thermoelastic stress measurement. Eng Fracture Mech. **183**, 1–12 (2017)
13. Paiva, V. Maneschy, R.J., Freire, J.L., Gonzáles, G.L.G., Vieira, R.D., Vieira, R.B.: Fatigue monitoring of a dented piping specimen using infrared thermography. PVP 2018, paper no. PVP 2018-84597, ASME pressure vessels & piping conference, Praga, Czech Republic. Proceedings of the PVP 2018, paper no. PVP 2018-84597, p. 1-7 (2018)
14. Paiva, V., Maneschy, R. J., Freire, J.L., Gonzáles, G. L. G. Vieira, R. D. Ribeiro, A.S. Almeida: Fatigue assessment and monitoring of a dented pipeline specimen, PVP 2019, paper no. PVP 2019-93663, ASME pressure vessels & piping conference, 2019, San Antonio, TX, USA. Proceedings of the PVP 2019, paper no. PVP 2019-93663, ASME pressure Vessels & Piping Conference, p. 1–8 (2019)
15. Paiva, V., Maneschy, R.J., Freire, J.L., Gonzáles, G.L. Vieira, G., Ribeiro, R.D., Almeida, A.S., Diniz, J.L.C: Fatigue monitoring of a dented pipeline specimen using infrared thermography, DIC and fiber optic strain gages, SEM conference and exposition on experimental and applied mechanics, Reno NV. Proceedings of the SEM Conference and Exposition on Experimental and Applied Mechanics, p. 1–10 (2019)
16. Paiva, V.E., Vieira, R.D., Freire, J.L.F: Fatigue properties assessment of API 5L Gr. B pipeline steel using infrared thermography. In: SEM Conference and Exposition on Experimental and Applied Mechanics, 2018, Greenville SC. Proceedings of the SEM Conference and Exposition on Experimental and Applied Mechanics. v. 1. p. 1–7 (2018)
17. Paiva, V.E.L.; Freire, J.L., Etchebehere, R.C.: Assessment of chain links using infrared thermography. In: CONAEND & IEV 2018–378, Congresso Nacional de Ensaios Não Destrutivos e Inspeção, 21 IEV Conferência Internacional sobre Evaluación de Integridad y Extensión de Vida de Equipos Industriales ABENDI, 2018, São Paulo. Anais do Conaend& IEV 2018, pp. 1–17 (2018)
18. Rajic, N., Rowlands, D.: Thermoelastic stress analysis with a compact low-cost microbolometer system. Quant Infrared Thermogr J. **10**(2), 135–158 (2013)
19. Weihrauch, M., Middleton, C., Greene, R., Patterson, E.: Low-cost thermoelastic stress analysis. In: Residual Stress, Thermomechanics & Infrared Imaging and Inverse Problems, pp. 15–19. Springer, Cham (2020)
20. Vieira. R.B.: Thermography Applied to the Study of Fatigue in Polycarbonate. Masters dissertation. PUC-Rio (2016)
21. https://www.flir.com/globalassets/imported-assets/document/flir-lepton-engineering-datasheet.pdf. Accessed 19 Feb 2020
22. https://www.flirmedia.com/MMC/THG/Brochures/RND_011/RND_011_US.pdf. Accessed 19 Feb 2020
23. Stress Photonics Inc.: DeltaTherm 2 Manual, v6(2016)
24. https://github.com/Kheirlb/purethermal1-uvc-capture. Accessed 21 Feb 2020
25. Vieira, R.B., Gonzáles, G.G., Freire, J.L.F.: Thermography applied to the study of fatigue crack propagation in polycarbonate. Exp. Mech. **58**(2), 269–282 (2018)
26. Díaz, F.A., Patterson, E.A., Yates, J.R.: Application of thermoelastic stress analysis for the experimental evaluation of the effective stress intensity factor. Frattura ed Integrità Strutturale. **7**(25), 109–116 (2013)
27. Paiva, V.E.L.: Modern Experimental Techniques with an Emphasis on Infrared thermography to the Assessment of Fatigue Components with Dents. PhD Thesis. PUC-Rio (2020)
28. Marsavina, L., Tomlinson, R.A.: A review of using thermoelasticity for structural integrity assessment. Fracture Struct Integr: Annals. **2014**, 8 (2014)
29. Stanley, P., Chan, W.K.: The determination of stress intensity factors and crack tip velocities from thermoelastic infra-red emissions. In: Proceedings of International Conference of Fatigue of Engineering Materials and Structures, pp. 105–114. IMechE, Sheffield (1986)